Available online at www.sciencedirect.com
ScienceDirect
Ceramics International 36 (2010) 947–954
CERAMICS INTERNATIONAL
www.elsevier.com/locate/ceramint

Synthesis of nanostructured material by mechanical milling and study on structural property modifications in $Ni_{0.5}Zn_{0.5}Fe_2O_4$

N.H. Vasoya, L.H. Vanpariya, P.N. Sakariya, M.D. Timbadiya, T.K. Pathak, V.K. Lakhani, K.B. Modi *

Department of Physics, Saurashtra University, Rajkot 360005, India

Received 19 September 2009; received in revised form 30 September 2009; accepted 22 October 2009
Available online 22 November 2009

Abstract

Mechanical milling induced structural property modifications in $Ni_{0.5}Zn_{0.5}Fe_2O_4$ spinel ferrite have been studied. We have observed two interesting phenomena (i) ''temperature diffuse scattering'' due to displacement of atoms from their mean position and (ii) appearance and gradual evolution of (4 2 0) plane in X-ray diffraction profiles and increase in average percentage disagreement between observed and calculated intensity ratios value, due to ''preferred grain orientation.'' Both these effects get prominent with milling time. The X-ray diffraction line intensity calculations revealed large B-site occupancy of Zn^{2+}-ions, mainly due to modified synthesis procedure employed. The grain orientation factor increases from 10.6% to 18.1% on milling. It is found that milling has marked influence on various parameters: lattice constant, grain size, stress–strain, surface area and energy.

Keywords: A. Milling; B. Grain size; D. Ferrites

1. Introduction

The research in nanoscience can be framed with three aims: to synthesize, understand and explore new nanomaterials and the related phenomena. Nanoparticles of spinel ferrites are of great interest in fundamental science for addressing relationship between physical properties and their crystal structure and chemistry. Due to their reduced sizes, these nanoparticles may possess novel and/or improved properties in comparison to the bulk materials. This has renewed interest to study different properties of pure and mixed spinel ferrite systems in nanocrystalline regime. A wide variety of techniques are being used to synthesize nanostructured materials including gas condensation, rapid solidification, electrodeposition, sputtering, crystallization of amorphous phases and chemical processing [1]. Mechanical attrition-ball milling is a technique which has also been used widely for preparation of nanostructured materials [2]. This has become a popular method to make nanocrystalline materials because of its simplicity and relatively inexpensive equipment needed, and the applicability to essentially all classes of materials. The major advantage often quoted is the possibility for easily scaling up to tonnage quantities of material for various applications. In fact contamination problem is often given as a reason to dismiss the method at least for some materials [1]. In the past the effectiveness of a milling process has been assessed in terms of changes in the particle shape, size and size distribution. Recently, it has become apparent that in order to characterize a powder more fully, account must be taken of the strain content induced during the milling process. Scores of research articles describing effect of grain size on magnetic properties of spinel ferrites synthesized by various chemical routes including ball milling are available in the literature. If we concentrate only on Ni–Zn ferrite system, which is one of the most studied spinel system, many research reports describing magnetic, electric and dielectric properties of $Ni_{1-x}Zn_xFe_2O_4$ ($x = 0.0$–1.0) ferrite system synthesized by various techniques are available in the literature [3–13]. A perusal of literature indicates that these particular aspects, i.e. mechanical milling induced strain and its effect on structural properties of $Ni_{0.5}Zn_{0.5}Fe_2O_4$ spinel ferrite have not been investigated in detail, though all other physical properties are decisively

* Corresponding author.
E-mail address: kunalbmodi2003@yahoo.com (K.B. Modi).

0272-8842/$36.00
doi:10.1016/j.ceramint.2009.10.024

dependent on structure, grain morphology and cation distribution in spinel ferrite system. We feel that this study will provide new dimension in the area of nano-sized ferrite materials and structure–property co relationship.

2. Experimental details

The bulk, about 20 g, spinel ferrite material with nominal composition $Ni_{0.5}Zn_{0.5}Fe_2O_4$, was prepared by the conventional ceramic route. The powders of α-Fe_2O_3, ZnO and NiO all 99.5% pure and supplied by Sigma Aldrich were thoroughly mixed in appropriate stoichiometry, wet ground and calcined at 900 °C for 24 h. Two more cycles of grinding and heating were used to ensure completer reaction. In pre-sintering process powder was kept at 950 °C for 18 h and slowly cooled to room temperature and in final sintering process powder was once again kept at 950 °C for 12 h and cooled to room temperature at the rate of 2 °C/min. The as prepared sample was milled up to 9 h using high energy planetary ball mill (Fritsch, Pulverisette 6) with tungsten carbide vials and balls. The milling intensity was 600 rotations per minute, and ball to powder ratio of 8:1 was chosen. A water was added to the container to improve particle mobility during milling. The milling process was interrupted after selected times (3 h, 6 h and 9 h) to take out small amount of powder, which were heated in air at 50 °C until completely dry. The stoichiometry of the powder sample was checked by energy dispersive analysis of X-rays (EDAX). The samples were characterized for single phase formation and the determination of structural parameters by X-ray diffractometry using Cu Kα radiation at 300 K. Microstructural characterization was performed by transmission electron microscopy (TEM), using a TECNAIK20 (Philips) microscope operated at 200 kV. For the TEM observations, the powder was first dispersed in amyl acetate by ultrasonication and then the suspension was dropped on a copper grid with a carbon film.

3. Results and discussion

3.1. Energy dispersive analysis of X-rays

It is well known that the high temperature, prolong sintering of spinel ferrite system containing cations such as Zn^{2+}, Li^{+}, Cd^{2+}, Ca^{2+} may results in loss of ingredient, produce oxygen vacancies and the resultant nonstoichiometric composition shows unexpected behaviour, that cannot be explain based on normal stoichiometry. Thus, it was essential to check the chemical stoichiometry of each composition. The result of EDAX (Table 1) confirms the expected stoichiometry. No trace of any impurity was found indicating the purity of the samples. It is also clear that there is no loss of any ingredient, this is mainly due to modified synthesis method employing with sintering temperature $\leq$950 °C. The EDAX results suggest that the precursors have fully undergone the chemical reaction to form the expected ferrite material. The reason for making EDAX characterization was to ratify the purity and surety of the chemical composition.

Table 1
EDAX results for un-milled sample of $Ni_{0.5}Zn_{0.5}Fe_2O_4$.

Element present	Expected	EDAX
	Concentration	
Ni	0.5	0.51 ± 0.02
Zn	0.5	0.48 ± 0.02
Fe	2.0	2.02 ± 0.02
O	4.0	3.98 ± 0.03

After stoichiometric confirmation by EDAX and formation of single phase, by X-ray diffraction pattern analysis, material was subject to high energy planetary ball milling. Initially the grains, most of which were a few micrometers in size, were of a uniform nature. As milling proceeded, however, these particles were continuously broken down, becoming irregular in shape, and a large distribution of fine 'chippings' could be observed. Prolonged treatment in the high energy planetary ball mill produced a marked and progressive colour changes in the $Ni_{0.5}Zn_{0.5}Fe_2O_4$ spinel ferrite sample. The powder, which was initially dark brown, becomes a lighter and lighter brown during milling.

3.2. X-ray diffraction pattern analysis

A first observation that one can made from raw X-ray diffraction patterns (Fig. 1), is that the intensity of the background scattering between lines increases, with milling time. This is called the ''temperature effect''. As a result of high energy ball milling high local temperature and pressure generated, this may result in the displacement of atoms from their mean position and leads to a partial breakdown of the conditions necessary for perfect destructive interferences between rays scattered at non-Bragg angles. This is called temperature diffuse scattering; it contributes only to the general background lines of the pattern and its intensity gradually increases with 2θ [14].

The room temperature (300 K) X-ray diffraction (XRD) patterns for the as prepared (un-milled; 0 h) and the ball milled samples for various milling times (3 h, 6 h, and 9 h) are illustrated in Fig. 2. The X-ray diffraction lines were found to be sharp, which makes the detection of any impurity phase easy. The indexing and lattice constant determination was carried out using powder-x software. All the samples are of single phase without detectable secondary phase within the limit of X-ray detection, which is typically 5%, and can be indexed with the face centered cubic (fcc) spinel structure of space group O_h^7 ($Fd3m$).

A careful examination of X-ray diffraction profiles (Fig. 2) revealed appearance of (4 2 0) diffraction line (which is also allowed fcc plane) between (4 0 0) and (4 2 2) planes for 3 h milled sample and its evolution with further milling time. It is found that (4 2 0) plane is totally absent for un-milled sample while its relative intensity increases from 2.5% for 3 h milled sample, 3.67% for 6 h milled sample to 8.28% for 9 h milled sample (Fig. 2). Here, it is important to note that (4 2 0) plane is generally not observed in X-ray diffraction patterns of spinel ferrite systems prepared by usual ceramic technique or fine particle ferrite systems synthesized by chemical routes. To best

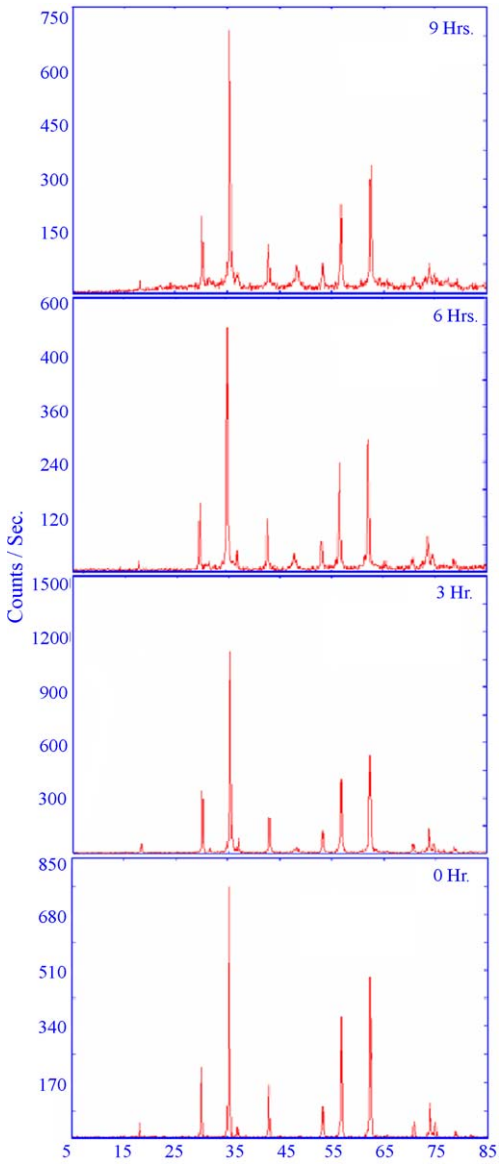

Fig. 1. X-ray diffractograms (raw data) for un-milled and milled samples of $i_{0.5}Zn_{0.5}Fe_2O_4$ spinel ferrite.

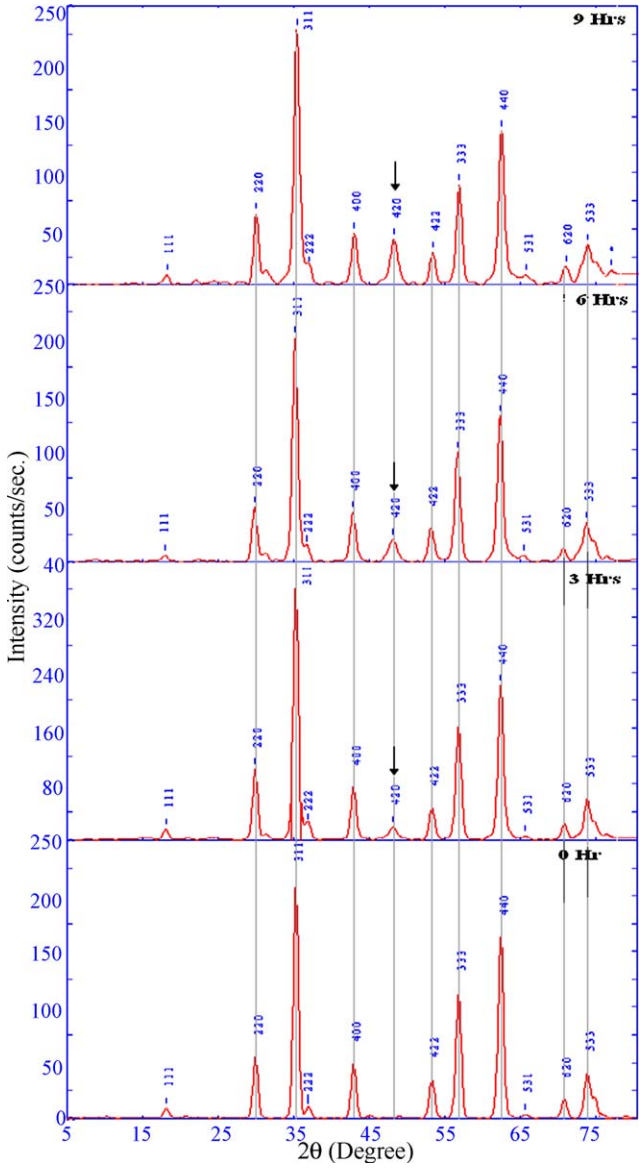

Fig. 2. X-ray diffraction patterns (fitted) of $Zn_{0.5}Ni_{0.5}Fe_2O_4$ spinel samples, at 300 K.

of our knowledge this is first observation of mechanical milling induced grain orientation in ferrite system. Earlier, for pure $NiFe_2O_4$ [3] and $ZnFe_2O_4$ [4] compositions, ball milled for about 40 h, (3 3 1) plane between (4 0 0) and (4 2 2) has been observed with very low intensity, but no emphasis was given. We feel that, appearance and gradual development of (4 2 0) plane for milled samples, is due to mechanically activated grain orientation. Each grain in a polycrystalline aggregate normally has a crystallographic orientation different from that of its neighbours. Considered as a whole, the orientations of all the grains may be randomly distributed in relation to some selected frame of reference, or they may tend to cluster, to a greater or lesser degree, about some particular orientation or orientations. Any aggregate characterized by the latter condition is said to have a preferred orientation, or texture, which may be defined simply as a condition in which the distribution of crystal orientations is nonrandom.

The degree of grain orientation in the sintered ceramics can be monitored by X-ray diffraction, using the X-ray orientation factor proposed by Lotgering [1]. As the amount of orientation increases, the 0 0 l X-ray diffraction peak increase and the non-0 0 l peaks decreases in intensity. Lotgering orientation factor is given by $L(f) = (p - p_0)/(1 - p_0)$, where p and p_0 are the ratios of the sums of intensities of the 0 0 l and $h\,k\,l$ peaks for the oriented and non-oriented patterns, respectively. We have observed expected variation of 0 0 l and $h\,k\,l$ peak intensity with orientation factor $L(f)$. The $L(f)$ is found about 10.6% for 3 h milled sample, for 6 h sample 15.7% and 18.1% for 9 h milled sample.

The lattice constant values were determined with an accuracy of ± 0.002 Å for different samples and are given in Table 2. It is found that lattice constant increases for un-milled samples to 6 h milled sample while for 9 h milled sample it shows sudden decrease.

Table 2
Lattice constant (a), ionic radius (r), grain size (D) for different samples of $Ni_{0.5}Zn_{0.5}Fe_2O_4$ spinel ferrite.

$Ni_{0.5}Zn_{0.5}Fe_2O_4$ sample	a (Å) ± 0.002 Å	r_A (Å)	r_B (Å)	a_{th} (Å)	D	FWHM (degree)	FWHM (radian) × 10^{-4}	Cos θ
		±0.002 Å						
0 h milled	8.4250	0.660	0.6675	8.3484	1.0 μm	–	–	–
3 h milled	8.4290	0.660	0.6675	8.3484	70 nm	0.1436	25.0470	0.95302
6 h milled	8.4390	0.665	0.6650	8.3494	55 nm	0.1715	29.9188	0.95329
9 h milled	8.4140	0.660	0.6675	8.3484	45 nm	0.2067	36.0555	0.95275

In Scherrer's formula: $\lambda = 0.15418$ nm, $b = 0.08^\circ$ (=1.3955 × 10^{-3} radian) were taken.

The change in lattice constant in general, be explained on the basis of (a) change in cation distribution (b) grain size effect, due to mechanical milling. Both these effects have been studied, for detailed investigation.

3.2.1. Cation distribution determination

In order to determine the distribution of cations among available tetrahedral (A-) and octahedral (B-) sites of spinel lattice, X-ray diffraction line intensity calculations were carried out using the formula suggested by Burger [15]:

$$I_{hkl} = |F_{hkl}|^2 P_m L_p$$

where $I_{h\,k\,l}$ is the relative integrated intensity, $F_{h\,k\,l}$ the structure factor, P_m the multiplicity factor and L_p is the Lorentz polarization factor (=1 + $\cos^2 2\theta/\sin^2\theta \cos\theta$).

According to Ohnishi and Teranishi [16], the intensity ratios of planes $I(2\,2\,0)/I(4\,4\,0)$ $I(4\,0\,0)/I(4\,2\,2)$, and $I(2\,2\,0)/I(4\,0\,0)$ are considered to be sensitive to the any change in cation distribution. The ionic configuration based on site preference energy values proposed by Miller [17] for individual cations in $Ni_{0.5}Zn_{0.5}Fe_2O_4$ composition, suggests that Zn^{2+} and Ni^{2+} ions preferentially occupy A- and B-sites respectively whereas Fe^{3+} ions occupy A- and B-sites.

An attempts to match the calculated values of plane ratio to observed ones with well accepted cation distribution: $(Zn_{0.5}{}^{2+}Fe_{0.5}{}^{3+})^A[Ni_{0.5}{}^{2+}Fe_{1.5}{}^{3+}]^BO_4{}^{2-}$ [18,19] surprisingly fails to large extent (Table 3). Similarly, presence of Ni^{2+}ions up to 20% on A-site [20] and Zn^{2+} ions up to 50% on B-site do not serve the purpose. We have found that for un-milled sample ~60% of Zn^{2+}-ions occupy B-site, with fairly good matching between observed and calculated intensity ratios value (Table 3). It is found that for 3 h and 9 h milled sample 60% of Zn^{2+} and for 6 h milled sample 50% of Zn^{2+} ions are present on the B-site. This is rather unexpected. It is worthwhile to note that as expected, Ni^{2+} ions occupy only B-site while occupancy of Fe^{3+} to the B-site varying from 60% to 62.5%, for 0 h to 9 h milled sample.

We feel that this is mainly due to modified synthesis procedure employed here for $Ni_{0.5}Zn_{0.5}Fe_2O_4$ composition. The percentage occupancy of Zn^{2+} ions (~60%) on B-site in the present case is much higher than that reported earlier by Oliver et al. [8]. It has been reported that for as produced powders of

Table 3
Comparison of X-ray diffraction line intensity ratios for $Ni_{0.5}Zn_{0.5}Fe_2O_4$.

$Ni_{0.5}Zn_{0.5}Fe_2O_4$ milling time	Cation distribution		$\frac{I(220)}{I(440)}$		$\frac{I(400)}{I(422)}$		$\frac{I(220)}{I(400)}$	
	A-site	B-site	Obs.	Cal.	Obs.	Cal.	Obs.	Cal.
0 h	$Zn_{0.5}Fe_{0.5}$	$Ni_{0.5}Fe_{1.5}$		0.283		8.898		0.328
	$Zn_{0.4}Ni_{0.1}Fe_{0.5}$	$Ni_{0.5}Zn_{0.1}Fe_{1.5}$		0.283		8.898		0.328
	$Zn_{0.4}Fe_{0.6}$	$Ni_{0.5}Zn_{0.1}Fe_{1.4}$		0.407		5.059		0.577
	$Zn_{0.3}Fe_{0.7}$	$Ni_{0.5}Zn_{0.2}Fe_{1.3}$		0.554		2.976		0.981
	$Zn_{0.2}Fe_{0.8}$	**$Ni_{0.5}Zn_{0.3}Fe_{1.2}$**	**0.760**	**0.724**	**1.706**	**1.774**	**1.667**	**1.645**
	$Zn_{0.1}Fe_{0.9}$	$Ni_{0.5}Zn_{0.4}Fe_{1.1}$		0.916		1.053		2.771
	$Zn_{0.21}Fe_{0.79}$	$Ni_{0.5}Zn_{0.29}Fe_{1.21}$		0.706		1.868		1.562
	$Zn_{0.19}Fe_{0.81}$	$Ni_{0.5}Zn_{0.31}Fe_{1.19}$		0.742		1.685		1.732
3 h	**$Zn_{0.2}Fe_{0.8}$**	**$Ni_{0.5}Zn_{0.3}Fe_{1.2}$**		**0.726**		**1.776**		**1.648**
	$Zn_{0.25}Fe_{0.75}$	$Ni_{0.5}Zn_{0.25}Fe_{1.75}$	**0.663**	0.638	**1.713**	2.298	**1.746**	1.273
	$Zn_{0.18}Fe_{0.82}$	$Ni_{0.5}Zn_{0.32}Fe_{1.18}$		0.762		1.601		1.828
6 h	$Zn_{0.2}Fe_{0.8}$	$Ni_{0.5}Zn_{0.3}Fe_{1.2}$		0.730		1.781		1.650
	$Zn_{0.24}Fe_{0.76}$	$Ni_{0.5}Zn_{0.26}Fe_{1.24}$		0.659		2.189		1.342
	$Zn_{0.25}Fe_{0.75}$	**$Ni_{0.5}Zn_{0.25}Fe_{1.25}$**	**0.525**	**0.642**	**1.940**	**2.305**	**1.227**	**1.275**
	$Zn_{0.26}Fe_{0.74}$	$Ni_{0.5}Zn_{0.24}Fe_{1.26}$		0.625		2.427		1.21
9 h	$Zn_{0.25}Fe_{0.75}$	$Ni_{0.5}Zn_{0.25}Fe_{1.25}$		0.460		2.293		1.269
	$Zn_{0.2}Fe_{0.8}$	**$Ni_{0.5}Zn_{0.3}Fe_{1.2}$**	**0.622**	**0.523**	**2.020**	**1.771**	**1.641**	**1.643**
	$Zn_{0.22}Fe_{0.78}$	$Ni_{0.5}Zn_{0.28}Fe_{1.22}$		0.497		1.964		1.481
	$Zn_{0.18}Fe_{0.82}$	$Ni_{0.5}Zn_{0.32}Fe_{1.18}$		0.550		1.597		1.822

$ZnFe_2O_4$ prepared through the low temperature (200 °C) supercritical sol gel drying method about 21% of Zn^{2+} cations and for 10 h milled sample 45% of Zn^{2+} ions occupy B-site [8,21]. It is consistent with 64% of Zn^{2+}-ions occupy B-site for 14 h milled sample of $ZnFe_2O_4$ [7]. The large redistribution of zinc cations into octahedral sites may be attributed to the ascendance in importance of simple geometric considerations over crystal energy and bonding effects in determining the site occupancy in these structurally disordered materials. Since ionic radius of Zn^{2+} ion (0.74 Å) is larger than the tetrahedral interstitial site dimension, the strong preference of Zn^{2+} ion for A-site was originally considered anomalous under equilibrium conditions. Later on the crystal energy calculations established that the tetrahedral site occupancy of zinc had a very high electrostatic stability [22]. It is, however, expected that the static structural disorder introduced by mechanical activation diminishes the relevance of the electrostatic energy compared to that of the large zinc ionic radii for site occupancy determination [8].

It is important to note that average percentage disagreement between observed and calculated intensity ratios value varies from 3.3% for un-milled sample to 5.9% for 3 h milled sample, 12.6% for 6 h and 9.5% for 9 h milled sample. This can be explained on the basis of grain orientation with milling. This is due to the fact that the cos θ portion of the Lorentz factor is valid only when the crystals making up the specimen are randomly oriented in space preferred orientation of the crystal grains causes radical disagreement between calculated and observed intensities and, when such disagreement exists, preferred orientation should be the first possible cause to be suspected [1]. This variation is quite consistent with the variation of strain (Table 4) with milling time.

In order to explain lattice expansion from 8.4250 Å for un-milled sample to 8.4390 Å for 6 h milled sample, we have calculated the value of the mean ionic radius per molecule of the A- and B-sites, (r_A and r_B, respectively), using the cation distribution for both the samples, using the relation [23]:

$$r_A = [C_{AZn} r(Zn^{2+}) + C_{AFe} r(Fe^{3+})]$$

$$r_B = (1/2)[C_{BZn} r(Zn^{2+}) + C_{BNi} r(Ni^{2+}) + C_{BFe} r(Fe^{3+})]$$

where $r(Zn^{2+})$, $r(Ni^{2+})$ and $r(Fe^{3+})$ are the ionic radii of Zn^{2+}(0.74 Å), Ni^{2++}(0.69 Å) and Fe^{3++}(0.64 Å) respectively, while C_{AZn}, C_{AFe} are the concentration of the Zn^{2+} and Fe^{3+} ions on A-site and C_{BZn}, C_{BNi}, and C_{BFe} are concentrations of Zn^{2+}, Ni^{2+} and Fe^{3+} ions on B-sites, respectively. It can be seen that (Table 2) r_A for un-milled sample is smaller than r_A for 6 h milled sample, due to replacement of larger Zn^{2+} ion from B-site to A-site, at the same time replacement of smaller Fe^{3+} ion from A-site to B-site, reduces r_B for 6 h milled sample. Of course, relative change in r_A is greater than r_B, but theoretically contribution of r_B is $\sqrt{3}$ times greater than r_A to the lattice constant value, thus overall increase in lattice constant value due to redistribution of cations is seems to be negligible.

It is known that there is a correlation between the ionic radius and the lattice constant. The lattice constant can be calculated theoretically by the relation suggested by Mazen et al. [24].

$$a_{th} = 8/3\sqrt{3}[(r_A + R_0) + \sqrt{3}(r_B + R_0)]$$

where R_0 is the radius of oxygen ions (1.32 Å). It is found that theoretically estimated lattice constant value (a_{th}) as well as previously reported experimental lattice constant values of 8.3937 Å [18], 8.3705 Å [25], 8.387 Å [12], etc. is much smaller than presently found experimental value of lattice constant. This may be due to presence of larger Fe^{2+}(0.74 Å) in the system. The formation of ferrous ion is quite probable in such systems. Apart from the phase identification, lattice parameter and grain size determination, X-ray diffraction pattern can also be used to study the lattice strain. The Bragg reflection peak (3 1 1) along with the corresponding Bragg angle (θ) and inter planer spacing (d) values, for all the samples is shown in Fig. 4 for comparison purpose.

It is found that the diffraction line shifts to lower angle for 3 h and 6 h milled samples with reference to un-milled sample while it shifts to higher angle for 9 h milled sample but does not otherwise change in intensity, as shown in Fig. 3. These observations suggest uniform strain has been produced due to mechanical milling in the samples. In the present case increase in lattice constant value from un-milled to 6 h milled sample may be due to the strong internal strains introduces during mechanical treatment causing increase in plane spacing d, results in the unit cell expansion and therefore in the 2θ positions of the diffraction lines. The formation and presence of Fe^{2+}-ions may also be the reason for lattice expansion, as Fe^{2+}–O bond length for A- and B-site is 1.995 Å and 2.12 Å respectively, while Fe^{3+}–O bond length is 1.865 Å and 2.02 Å for A- and B-site, respectively [18].

3.2.2. Grain size determination

The average grain diameter (D) for ball milled samples was calculated from the broadening of the respective high intensity (3 1 1) peak using the Debye Scherrer formula:

$$D = \frac{K\lambda}{B\cos\theta}$$

Here, λ is the wave length of the Cu Kα radiation (=0.15418 nm), constant K (=0.9), is related both to the

Table 4
Stress–strain parameters for milled samples.

$Ni_{0.5}Zn_{0.5}Fe_2O_4$ sample	$\frac{\Delta d}{d} \times 10^{-4}$	Tensile stress $\times 10^5$	Compressive stress $\times 10^5$	Tensile strain OR compressive strain $\times 10^{-4}$
3 h milled	03.145	192.3	141.8	01.573
6 h milled	29.800	1839.8	1316.1	14.900
9 h milled	27.680	1734.2	1230.0	13.840

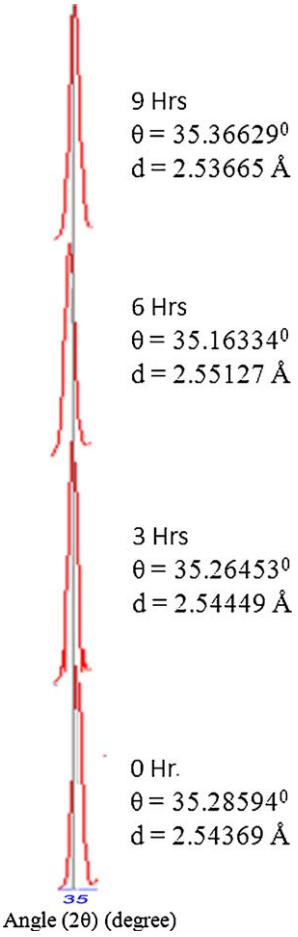

Fig. 3. X-ray diffraction peak (3 3 1) for different $Ni_{0.5}Zn_{0.5}Fe_2O_4$ samples.

crystallite shape and the way in which B and D are defined. B is the contribution to the XRD peak width due to the small size of crystallites in radians. The contribution must separate out from the measured line width B_m which includes instrumental broadening b, always present irrespective of the particle size. For this, one can record XRD pattern of a well crystallized, bulk, standard material such as silicon powder under identical geometrical conditions and measure the peak width b. The broadening parameter B is obtained from the relation:

$$B = (B_m^2 - b^2)^{1/2}$$

The average grain size reduces from 70 nm for 3 h milled sample to 45 nm for 9 h milled sample (Table 2). Size of the grain decreases as the milling time increases because the kinetic energy generated by the series of collisions among balls is transferred to the system. The grain size when calculated at different θ values was at variance, indicating the presence of strain.

While X-ray diffraction (XRD) pattern analysis gives the crystal structure and average grain size, transmission electron microscopy (TEM) shows the grain morphology and its size distribution. Fig. 4 shows typical transmission electron micrograph of the 3 h milled sample. The grain size estimated from TEM is slightly greater than the grain size estimated from

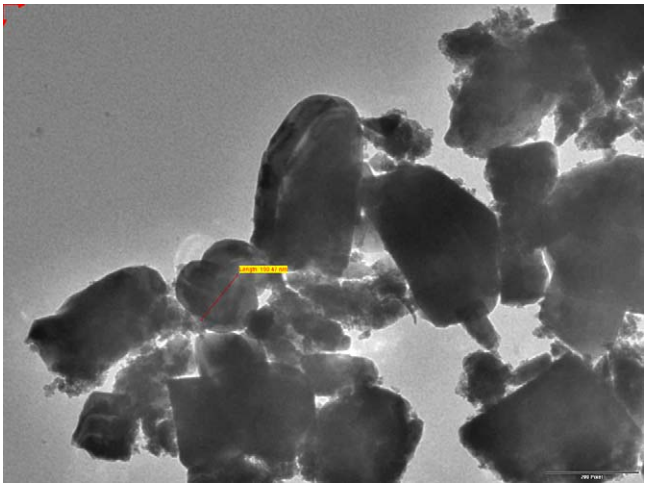

Fig. 4. Transmission electron micrograph for 3 h milled sample of $Ni_{0.5}Zn_{0.5}Fe_2O_4$.

XRD for all the samples. This is because X-ray diffraction gives the information of crystalline region only and the contribution from the amorphous grain surface does not contribute. On the other hand TEM gives the complete picture of the nanoparticles.

It follows that for 3 h and 6 h milled samples, there would be unpaired electronic orbital at the outer surface of each particle. This roughly parallel array of surface dipoles would repel each other and result in a larger value of the equilibrium lattice constant than in the bulk crystal [26]. The probable reason for reduction in lattice constant value for 9 h milled sample could be the presence of lattice defects and its influence on the nanoparticles, especially on the surface.

3.3. Stress–strain determination

The variation in strain ($\Delta d/d$), equivalent to a fractional variation in plane spacing, has been calculated for milled samples by taking into account 'd' spacing value of most intense (3 1 1) peak and given in Table 4. This value of $\Delta d/d$ however, includes both tensile and compressive strain and must be divided by two to obtain the maximum tensile strain alone, if

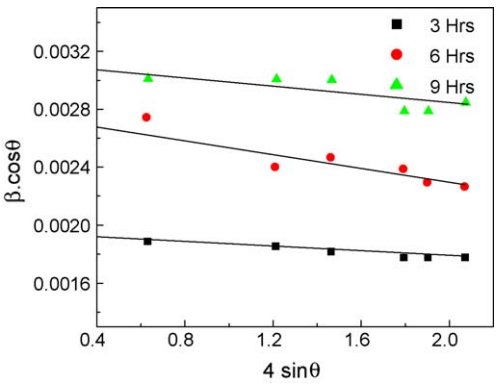

Fig. 5. Strain graphs for 3 h, 6 h, and 9 h, milled samples of $Ni_{0.5}Zn_{0.5}Fe_2O_4$ spinel ferrite.

Table 5
Strain (ε), bulk density (ρ), surface area (S) and equivalent surface free energy for different samples of $Ni_{0.5}Zn_{0.5}Fe_2O_4$ spinel ferrite.

$Ni_{0.5}Zn_{0.5}Fe_2O_4$ sample	$\varepsilon \times 10^{-4}$ (W–H)	$\langle \varepsilon^2 \rangle^{1/2} \times 10^{-5}$	D (W–H)	ρ (g/cm^3)	S (m^2/g)	Equivalent surface free energy (10^{-3} cal/g)
0 h milled	–	–	2.5 μm	4.53	0.53	0125.6
3 h milled	1.0	7.07	80 nm	4.50	16.67	3950.8
6 h milled	3.2	22.62	58 nm	4.37	23.67	5609.8
9 h milled	4.3	30.40	48 nm	4.38	27.40	6493.8

these two are assumed equal. The maximum strain so found can than be multiplied by the Young's modulus (E) and bulk modulus (B) respectively, to give the maximum stress present. Initially, the strain rapidly increases from 3 h milled to 6 h milled sample and then slowly decreases for 9 h milled sample (Table 4). Earlier, for many metals it has been observed that, the strain rises with decreasing grain size, reaches a maximum and then decreases to low values for the smallest nanocrystalline grain sizes [1], as in the present case. Stress relaxation may be responsible for the maxima. In the early stage of ball milling, the strain increases due to the increasing defect density.

The grain size and microstrain developed during the milling process were also deduced from the X-ray diffraction line broadening (B) using the analysis described by Williamson and Hall (W–H) [27]

$$B\cos\theta = \varepsilon(4\sin\theta) + \frac{\lambda}{D}$$

where B (FWHM in radian) is measured for different XRD lines corresponding to different planes, ε is the strain developed and D is the grain size. The equation represents a straight line between 4 sin θ (X-axis) and B cos θ (Y-axis). The slope of line gives the strain (ε) and intercept (λ/D) of this line on the Y-axis gives grain size (D).

Fig. 5 shows 4 sin $\theta \rightarrow B$ cos θ lines for all the three milled samples. All exhibit the scatter of points known as a 'deviation pattern' which is typical of a deformed face centered cubic materials [28]. The grain sizes calculated from this graph is in reasonable agreement to those calculated from Scherrer's formula. Strain continues to increase with an increase in milling time. Since the strain effect is cumulative with time it probably occurs initially in the surface regions of the grains, but as milling proceeds and the grains become smaller, strain becomes evident throughout each grain. The root mean square (rms) atomic level strain $\langle \varepsilon^2 \rangle^{1/2}$ within the particles are also included in Table 5. Strain values are also consistent with those calculated from d-spacing values. The grain size determined from W–H formula is slightly higher than those calculated using Scherrer's formula (Table 2). The difference in the values is due to the fact that in Scherrer's formula strain component is assumed to be zero and observed broadening of diffraction peak is considered as a result of reducing grain size only.

Attempt has been made to calculate surface area (S) and equivalent surface free energy for all the samples. Assuming all the particles to be spherical, the specific surface area in meter square per gram is given by:

$$S = \frac{6000}{D\rho}$$

where D is the diameter of the particle in nm and ρ the density of the particle in g/cm^3. The specific surface area (Table 5) of the particle increases as the grain size decreases.

The surface free energy calculated assuming the grains to be spheres with a surface energy of 1000 erg/cm^2 [29], increases with decreasing grain size. In the case of nanoparticles, surface atoms are not bonded to the maximum number of nearest neighbours, and are therefore in a higher energy state than the atoms at interior positions. The bonds of these surface atoms that are not satisfied give rise to a surface energy. In the field of nanomagnetism this surface energy plays very crucial role.

4. Conclusions

Summing up the study on the mechanical milling induced structural modifications in $Ni_{0.5}Zn_{0.5}Fe_2O_4$ spinel ferrite, leads to conclude that:

(i) milling induced strain displaced atoms from their mean position, results in ''temperature diffuse scattering'' effect.
(ii) the appearance and evolution of (4 2 0) plane for milled samples as well as increase in average percentage disagreement between observed and calculated intensity ratio values with milling time is due to preferred orientation of grains.
(iii) occupancy of Zn^{2+}-ions at B-sites for all the samples is about 50–60% confirmed by X-ray intensity calculations mainly due to modified synthesis procedure employed.
(iv) maximum stress and strain have been observed for 6 h milled sample after that it levels off, the parameters like lattice constant, grain size, surface area and surface energy are greatly influenced by milling.

Based on above facts it is clear that mechanical milling induced strain and its effect on structural properties leads to some interesting phenomena. These may help to understand other physical properties in depth.

Acknowledgment

One of the authors (KBM) is thankful to UGC New Delhi for providing financial assistance in the form of UGC research award scheme-2009.

References

[1] C.C. Koch, Synthesis of nanostructured materials by mechanical milling: problems and opportunities, Nanostruct. Mater. 9 (1–8) (1997) 13–22; F.K. Lotgering, Topotactical reactions with ferrimagnetic oxides having hexagonal crystal structures-I, J. Inorg. Nucl. Chem. 9 (1959) 113–116.

[2] B.P. Richards, A.C. Greenham, Strain induced in yttrium iron garnet by various milling treatments, Br. J. Appl. Phys. (J. Phys. D) 2 (1) (1968) 1297–1302.

[3] N. Ponpandian, P. Balaya, A. Narayanasamy, Electrical conductivity and dielectric behaviour of nanocrystalline $NiFe_2O_4$ spinel, J. Phys.: Condens. Matter 14 (2002) 3221–3237.

[4] N. Ponpandian, A. Narayanasamy, Influence of grain size and structural changes on the electrical properties of nanocrystalline zinc ferrite, J. Appl. Phys. 92 (5) (2002) 2770–2778.

[5] N. Shivakumar, D. Narayanasamy, N. Ponpandian, G. Govindraj, Grain size effect on the dielectric behavior of nanostructured $Ni_{0.5}Zn_{0.5}Fe_2O_4$, J. Appl. Phys. 101 (2007) 084116–84126.

[6] A.K.M. Akther Hossain, S.T. Mahmud, M. Seki, T. Kawai, H. Tabala, Structural, electrical transport and magnetic properties of $Ni_{1-x}Zn_xFe_2O_4$, J. Magn. Magn. Mater. 312 (2007) 210–219.

[7] J.Z. Jiang, P. Wynn, S. Morup, T. Okada, F.J. Berry, Magnetic structure evolution in mechanically milled nanostructured $ZnFe_2O_4$ particles, Nanostruct. Mater. 12 (1999) 737–740.

[8] S.A. Oliver, V.G. Harris, H.H. Hamdeh, J.C. Ho, Large zinc cation occupancy of octahedral sites in mechanically activated zinc ferrite powders, Appl. Phys. Lett. 76 (19) (2000) 2761–2763.

[9] R.V. Mangalaraja, L.S. Thomas, S. Anantha Kumar, P. Manohar, P. Camirru Carlos, Effect of composition on initial permeability of $Ni_{1-x}Zn_xFe_2O_4$ prepared by flash combustion technique, Mater. Sci. Eng. A 476 (2008) 234–239.

[10] M. George, A.M. John, S.S. Nair, P.A. Joy, M.R. Anantharaman, Finite size effects on the structural and magnetic properties of sol–gel synthesized $NiFe_2O_4$ powders, J. Magn. Magn. Mater. 302 (2006) 190–195.

[11] A. Verma, D.C. Dube, Processing of nickel–zinc ferrites via the citrate precursor route for high-frequency applications, J. Am. Ceram. Soc. 88 (2005) 519–523.

[12] A. Verma, O.P. Thakar, C. Prakash, T.C. Goel, R.G. Mendiratta, Temperature dependence of electrical properties of nickel–zinc ferrites processed by the citrate precursor technique, Mater. Sci. Eng. B. 116 (2005) 1–6.

[13] C.N. Chinnasamy, A. Narayanasamy, N. Ponpandian, K. Chattopadhyay, K. Shinoda, B. Jeyadevan, K. Tohji, K. Nakatsuka, T. Furubayashi, I. Nakatani, Mixed spinel structure in nanocrystalline $NiFe_2O_4$, Phys. Rev. B 63 (2001) 184108–184114.

[14] B.D. Cullity, Elements of X-ray Diffraction, 2nd edn., Addison Wesley Pub. Co., Reading, MA, 1978.

[15] M.J. Burger, Crystal Structure Analysis, Wiley, NY, 1960.

[16] H. Ohinishi, T. Teranishi, Crystal distortion in copper ferrite–chromite series, J. Phys. Soc. Jpn. 16 (1961) 35–43.

[17] A. Miller, Distribution of cations in spinels, J. Appl. Phys. 30 (1959) 24S–25S.

[18] C.M.B. Henderson, J.M. Charnook, D.A. Plant, Cation occupancies in Mg, Co, Ni, Zn, Al ferrite spinels: a multi-element EXAFS study, J. Phys. Condes. Matter 19 (2007) 076214–076239.

[19] S. Gubbala, H. Nathani, K. Koizol, R.D.K. Mishra, Magnetic properties of nanocrystalline Ni–Zn, Zn–Mn, and Ni–Mn ferrites synthesized by reverse micelle technique, Physica B 348 (2004) 317–328.

[20] T. Shimada, T. Tachibana, T. Nakagawa, T.A. Yamamota, Site occupation study of $ZnFe_2O_4$ and $NiFe_2O_4$ by far-infrared reflectivity, J. Alloys Compd. 379 (2004) 122–126.

[21] H.H. Hamdeh, J.C. Ho, S.A. Oliver, R.J. Willey, G. Oliveri, G. Busca, Magnetic properties of partially-inverted zinc ferrite aerogel powders, J. Appl. Phys. 81 (1997) 1851–1857.

[22] V.A.M. Brabers, in: K.H.J. Buschow (Ed.), Handbook of Magnetic Materials, vol. 8, Elsevier Science B.V., Amsterdam, 1995, pp. 195–204.

[23] A. Globus, H. Pascard, V. Cagan, Distance between magnetic ions and fundamental properties in ferrites, J. Phys. Suppl. 438 (C-1) (1977) 163–168.

[24] S.A. Mazen, M.H. Abdallah, B.A. Sabrah, H.A.M. Hasham, The effect of titanium on some physical properties of $CuFe_2O_4$, Phys. Status Solidi A134 (1992) 263–271.

[25] K.J. Standly, Oxide Magnetic Materials, Clarendom Press, Oxford, 1972.

[26] A. Pushan, V.R. Palkar, S. Chattopadhyay, M. Multani, Effect of crystal size reduction on lattice symmetry and co operative proportion, Phys. Rev. B 51 (a) (1995) 6135–6138.

[27] G.K. William, W.H. Hall, X-ray line broadening from field aluminum and wolfram, Acta Metall. 1 (1) (1953) 22–31.

[28] D. Lewis, H. Pearson, The milling of soft metals to produce very large lattice strains, Appl. Phys. Lett. 7 (12) (1965) 316–318.

[29] E. Ryshkewitch, Oxide Ceramics Physical Chemistry and Technology, Academic Press, N.Y., 1960.